Heat Transfer and Adhesion Study for the FFF Additive Manufacturing Process

Arthur Lepoivre, Nicolas Boyard, Arthur Levy, Vincent Sobotka

Available online at www.sciencedirect.com

ScienceDirect

Procedia Manufacturing 00 (2019) 000–000

Procedia MANUFACTURING

www.elsevier.com/locate/procedia

23rd International Conference on Material Forming (ESAFORM 2020)

Heat Transfer and Adhesion Study for the FFF Additive Manufacturing Process

Arthur Lepoivre[a,b] *, Nicolas Boyard[a], Arthur Levy[a], Vincent Sobotka[a]

[a] *Université de Nantes, CNRS, Laboratoire de thermique et énergie de Nantes, LTeN, UMR 6607, F-44000 Nantes, France*

[b] *Institut de Recherche Technologique Jules Verne,44340 Bouguenais, France*

* Corresponding author: arthur.lepoivre@univ-nantes.fr

Abstract

Additive manufacturing is becoming more and more important today by offering very advantageous opportunities. It gives the ability to manufacture parts with complex geometry, without the need of specific tools. This work focuses on fused filament fabrication process. It consists in melting the polymer, and extruding it through a nozzle to create a structure defined by a toolpath. The extruded filament solidifies while cooling.

One of the major drawbacks of this process is the poor mechanical properties of the parts compared to thermoplastic injection. This is related to (i) the porosities between deposited filaments and (ii) the limited adhesion between deposited layers. This adhesion phenomenon is thermally driven by the molecular mobility of the polymer chains. The objective of this work is to understand, model and quantify heat exchanges in the process, in order to define the process window leading to optimal mechanical resistance of the parts.

With this aim, a laboratory-scale instrumented 3D printing machine has been designed and manufactured. This bench is thermally controlled. Polymer and environment temperatures can be measured with an infrared camera, pyrometer and thermocouples instrumentation. In parallel, a numerical model has been developed to predict the influence of the process parameters on the cooling and adhesion. For this purpose, thermal properties have been characterized. A sensitivity analysis quantifies the most relevant properties to measure and control accurately and a comparison between numerical and experimental results validates the approach.

Keywords: additive manufacturing ; Fused Filament Fabrication ; heat transfer ; adhesion ; infrared measurement

1. Introduction

Additive manufacturing, or 3D printing, is the generic term for several material processes, such as Fused Filament Fabrication (FFF), StereoLithograPhy (SLA) or Selective Laser Melting (SLM). According to the Wohlers Report 2019 [1], all additive manufacturing products and services would represent $15.8 billion revenue in 2020 and $35.6 billion in 2024. This work focuses on the FFF process that has a lot of applications in aeronautic, automotive, health and prototyping industries. In this process, 3D parts are manufactured by extruding a melted thermoplastic filament through a nozzle. The toolpath of the nozzle is previously designed by software in order to create the part. The filament is heated by the extrusion unit that brings the polymer in a viscous or molten state. After deposition, the filament cools down with its environment and solidifies, allowing the addition of new layers. This process offers advantage of producing parts with complex geometry, with a wide choice of materials without requiring the use of a molding cavity. However, this process has several drawbacks: (a) the size of the manufactured parts are limited, (b) the manufacturing time remains long (c) the

mechanical properties are lower compared to parts produced with other processes as injection for example. This work focuses on this poor mechanical trade-off.

At the macroscopic scale, in order to achieve a good adhesion, it is necessary to find the compromise about the adequate processing temperatures (air temperature inside the printing atmosphere and nozzle temperature). As illustrated in Fig. 1, the temperature must be high enough to develop a sufficient interface healing of the filaments. But this temperature should not be too high to avoid structure collapse because of low viscosity or thermal degradation/chemical aging of the extruded polymer. To find precisely the limit of this optimal processing area, the thermal history needs to be predicted accurately.

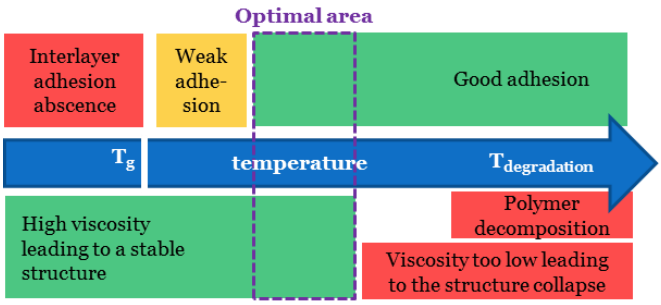

Fig. 1. Polymer printability rules for FFF process.

At the filament scale, the decrease of mechanical properties is due (i) to the macro-porosities inside the part due to the circular shape of the filaments and (ii) to the poor adhesion at the interface of adjacent filaments.

(i) Macro-porosities: This first phenomenon can be associated to the coalescence of two polymer spheres as described by Frenkel's model [2], [3] and analytical solutions were proposed for cylinders [4]–[6]. Frenkel's model has been used in the literature by authors working on additive manufacturing process [7]–[13]. The coalescence process is described by the angle of coalescence in degree θ, which follows the evolution rate:

$$\frac{d\theta}{dt} = \frac{\sigma(T)}{a_0 \cdot \mu(T)} \cdot \frac{2^{-5/3}\cos(\theta)\sin(\theta)\cdot(2-\cos(\theta))^{1/3}}{(1-\cos(\theta))\cdot(1+\cos(\theta))^{1/3}} \quad (1)$$

where σ is the surface tension in N/m; a_0 the initial radius of the cylinder in m; μ the viscosity in Pa.s and T the temperature of the polymer in K. Note that surface tension and viscosity are two thermally dependent properties.

(ii) Adhesion: The second phenomenon can be empirically defined by the reptation theory by De Gennes [14]. It has been studied in the polymer processing literature [15], [16] and can be modeled by the degree of healing D_h, which evolution rate follows:

$$D_h(t) = \left(\frac{t}{t_R(T)}\right)^{1/4} \quad (2)$$

where t_R is the temperature dependent reptation time of the polymer, which can be identified with a rheological study.

Coalescence and reptation phenomena are both thermally-driven, through the variation of the temperature dependent properties (surface tension σ, viscosity μ and reptation time t_R). It justifies the importance to predict the accurate thermal history of the polymer during its printing. This is the aim of the present work.

There are several heat transfers phenomena during the FFF process, as illustrated in Fig. 2: (1) heat brought by the extruder, often with a heating resistance, (2) convective cooling of the filament with the air, (3) heat exchanges between the adjacent filaments, (4) heat brought by the support plate, (5) radiative losses and (6) heat source from the exothermal crystallization for semi-crystalline polymers.

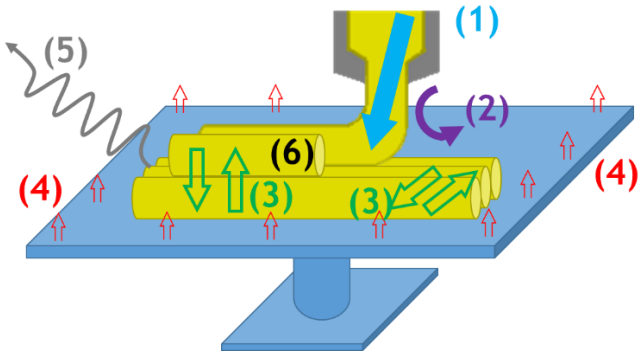

Fig. 2. At least 6 different heat transfer phenomena are identified in the FFF process.

In the 90's, heat transfer in the FFF process was studied in the literature, with a 1D analytical model and 2D numerical model by Yardimci [17], [18] and was used to predict filament temperature evolution [8], [12]. In 2000 and 2003, Rodriguez and Thomas proposed a 2D analytical model [19], [20]. These two models were compared with experimental data (thermocouple between two layers) by Sun *et al.* [7] in Fig. 3.

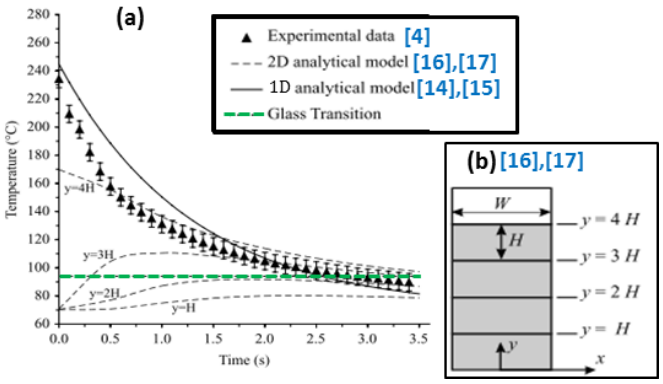

Fig. 3. (a) Comparison of the heat transfer model existing in the literature of FFF process and (b) geometry for the 2D analytical model. Adapted from [7].

The 1D analytical model seems to over-estimate the experimental temperature evolution, but has the good trend. The 2D analytical model ($y = 4H$ for the last filament extruded) seems to best fit the measurements, but only after 0.5s. For information, the glass transition T_g of ABS is also plotted in the figure. Adhesion develops while temperature is above T_g.

Some authors modelled the deformation of the extruded filament [13], [21]–[24]. It appears to be very temperature dependent. This work will focus on accurate prediction of adhesion and heat transfer.

The final objective of the work consists in describing and controlling FFF process with high temperature material, more specifically PEKK material reinforced or not with short carbon fibers, for aeronautic applications. The experimental development was developed initially on ABS, for its greater ease of implementation.

In order to understand and quantify the heat transfer and adhesion phenomena during the FFF process, two methods are used. First, an experimental bench has been designed and fabricated, with the objective to measure the temperature field of the polymer during its printing with infrared (IR) technology. The second method is a simulation model developed with COMSOL Multiphysics® v5.4 to predict temperature evolution and degree of healing.

2. Methodology

2.1. Instrumented bench

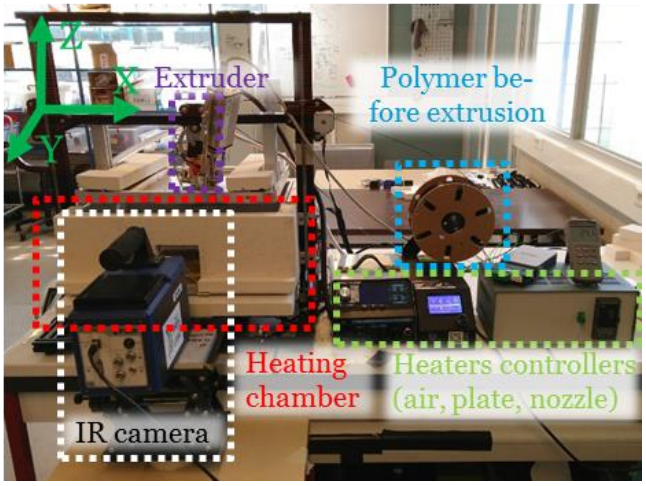

Fig. 4. Experimental bench showing the heated chamber for 3D printing of high temperature polymers and the infrared camera for temperature measurements.

Bench description:

The experimental bench is a modified commercial 3D-printer CR-10 from Creality3D, based on the open-source Prusa i3 structure, as shown in Fig. 4. The main issue is to measure the temperature *in situ* at the scale of a single filament (~1mm), during the part fabrication. With the perspective of studying high performance thermoplastic (PAEK family), the commercial printer was upgraded to reach the temperature levels for this polymer family: up to 400°C.

A 500W heating plate system was built, to reach plate temperature around 250°C. The extruder was changed, for full-metal unit, with a water-cooling closed circuit system. A closed insulated chamber maintains the part in a 200°C atmosphere. It does not block the three translation moving system of the 3D-printer inside the chamber. Electronics and mechanical parts are kept outside the chamber. This heating chamber is mandatory for printing polymers like PEKK.

Temperature measurements:

Thermal instrumentation consists in an infrared camera SC7500 InSb from FLIR and a modified pyrometer PYROSPOT DPE 10M from DIAS Infrared Systems. PEKK material was characterized to determine its emissivity versus wavelength. The pyrometer and IR camera wavelengths were chosen accordingly and operate both within the wavelength range 3.7 – 5.1 µm. FTIR spectrometer was used, on the 1.4-17.9 µm wavelength range, with KBr separator, LN MCT Mid 2x2mm detector and golden integrating sphere at ambient temperature. Complementary work performed by another team in the project indicated the absence of thermal influence on the emissivity, for a fixed wavelength. We supposed the same constant behavior for the wavelengths we use for IR measurement technology. Absorbance was deduced after measurement of normal-hemispheric transmittance and reflectance.

Additionally, the smallest target size for commercial pyrometer is $\emptyset_{pyrometer} = 0.6\ mm$. Thus, we had to adapt the bench, and use a bigger nozzle, which was $\phi_{nozzle} = 1\ mm$, than usual in the additive manufacturing process.

Procedure:

A simple geometry was 3D-printed part in ABS and PEKK: a 60x2.2x50 mm wall part, with a single filament in the thickness along the z-axis, as illustrated in Fig. 5.

Obviously, IR camera and pyrometers devices need to be kept out of the printing chamber because of the temperature level. Two infrared transparent windows made of CaF_2 are positioned on the side and the top of the chamber. Qualitative measurements were performed with infrared camera for ABS, without temperature determination because calibration was not performed for the used objective yet. Quantitative measurements were given by the pyrometer for ABS and PEKK. Polymer emissivity were taken as $\varepsilon = 0.91$ for ABS as reported in the literature [25] and $\varepsilon = 0.94$ for PEKK, measured from spectroscopy characterization over the adequate wavelength range. The measurement device was pointing normal to the wall length as indicated in Fig. 5:

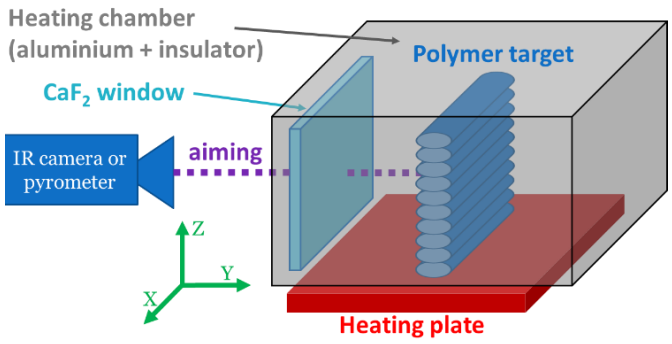

Fig. 5. Experimental set-up. A single filament wall was 3D printed. The pyrometer measures the temperature from the side in situ.

2.2. Heat transfer modeling for FFF process

Let's consider the domain Ω represented in Fig. 6. In this domain, heat transfer equations can be described by the following set of equations.

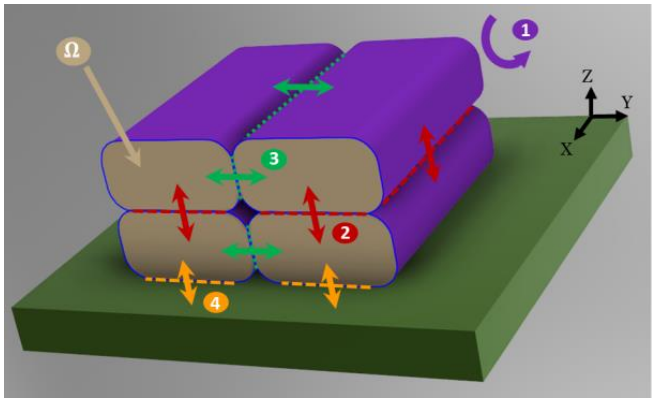

Fig. 6. Geometry and boundary conditions used in the heat transfer model.

In Ω domain:

$$\rho C_p \left(\frac{\partial T}{\partial t} + \boldsymbol{u} \cdot \boldsymbol{\nabla} T\right) = \nabla \cdot \left(\boldsymbol{k} \cdot \boldsymbol{\nabla} T\right) + Q_{\text{crystallization}} \quad (3)$$

where ρ is the density, C_p the specific heat, u the polymer velocity and $\boldsymbol{k}$ the conductivity tensor and $Q_{\text{crystallization}}$ a source term for the crystallization effects.

Boundary condition on 1:

A heat transfer coefficient models the convection cooling:

$$-k\vec{\nabla}\mathrm{T} \cdot \vec{n} = \mathrm{h}_{\text{convection}} \cdot (T - T_{chamber}) \quad (4)$$

with $h_{convection}$ the convection heat transfer coefficient, the radiative effects are neglected.

Interface conditions:

Thermal contact resistances (TCR) are assumed on all the internal boundaries. Thus the heat flux through these boundaries writes:

$$-k\vec{\nabla}\mathrm{T} \cdot \vec{n} = \frac{1}{TCR_{filament\,\backslash z}}(T^+ - T^-) \quad \text{on } 2 \quad (5)$$

$$-k\vec{\nabla}\mathrm{T} \cdot \vec{n} = \frac{1}{TCR_{filament\,\backslash y}}(T^+ - T^-) \quad \text{on } 3 \quad (6)$$

$$-k\vec{\nabla}\mathrm{T} \cdot \vec{n} = \frac{1}{TCR_{support}}(T^+ - T^-) \quad \text{on } 4 \quad (7)$$

where T^+ and T^- are the temperatures on both sides of the interface.

Initial conditions:

At initial time, the temperature in each domain is supposed to be known and uniform:

$$T(t=0) = T_{extrusion} \quad \text{on the polymer just extruded} \quad (8)$$

$$T(t=0) = T_{filaments} \quad \text{on the previously extruded filaments} \quad (9)$$

$$T(t=0) = T_{support} \quad \text{on the support plate} \quad (10)$$

As long as the exothermal enthalpy of the crystallization is low, this term can be neglected, with $\Delta H_{crystallization} < 40\ J/g$ for PEKK [26] and with no crystallization for ABS (amorphous). Moreover, the thermal conductivity of the material $\overline{\overline{k}}$ is considered as constant, but it can be anisotropic for fiber reinforced material. As there is not fluid flow inside the extruded filament, so $u = 0$.

From the equation (3) and with these assumptions, the simplified heat transfer in 3D can be written:

$$\frac{\partial T}{\partial t} = \frac{k_x}{\rho C_p}\frac{\partial^2 T}{\partial x^2} + \frac{k_y}{\rho C_p}\frac{\partial^2 T}{\partial y^2} + \frac{k_z}{\rho C_p}\frac{\partial^2 T}{\partial z^2} \quad (11)$$

The diffusion term in the x direction can also be neglected such that the problem reduces to a 2D model. In order to check the accuracy of this simplification, a dimensional analysis is performed, for a filament of length L_x, width L_y and thickness L_z. Dimensionless variables are defined as:

$$T^* = \frac{T - T_{chamber}}{T_{extrusion} - T_{chamber}} \quad (12)$$

$$x^* = \frac{x}{L_x}\ ;\ y^* = \frac{y}{L_y}\ ;\ z^* = \frac{z}{L_z}\ ;\ t^* = \frac{t}{\tau_c} \quad (13)$$

$$[T^*; x^*; y^*; z^*] \in [0;1] \quad ; \quad t^* \in [0; +\infty] \quad (14)$$

Three Fourier numbers Fo_x, Fo_y and Fo_z are then introduced. They characterize the ratio between the conductivity term over the inertia term, and take into account a characteristic time on the order of magnitude $\tau_C = 1s$, corresponding to the process time:

$$Fo_i = \frac{k_i}{\rho C_p} \cdot \frac{\tau_c}{{L_i}^2} \qquad \text{With } i = x, y \text{ or } z \quad (15)$$

The dimensionless heat-transfer equation is obtained as:

$$\frac{\partial T^*}{\partial t^*} = Fo_x \frac{\partial^2 T^*}{\partial x^{*2}} + Fo_y \frac{\partial^2 T^*}{\partial y^{*2}} + Fo_z \frac{\partial^2 T^*}{\partial z^{*2}} \quad (16)$$

Very early during the printing, the length of the filament L_x becomes much larger than the filament section dimensions L_y and L_z. Thus:

$$Fo_x \ll Fo_y \text{ and } Fo_x \ll Fo_z \quad (17)$$

As a matter of fact, usually in printed parts, $L_y > L_z$. Therefore, the condition becomes:

$$t > \sqrt{10\frac{k_x}{k_y}} \cdot \frac{L_y}{v_{printing}} \sim 0.01s \quad (18)$$

Where $v_{printing}$ is the printing velocity, the condition $Fo_x < 0.1\ Fo_y < 0.1\ Fo_z$ is fulfilled.

Under these assumptions, the heat transfer equation reduces to:

$$\frac{\partial T^*}{\partial t^*} = Fo_y \frac{\partial^2 T^*}{\partial y^{*2}} + Fo_z \frac{\partial^2 T^*}{\partial z^{*2}} \quad (19)$$

With our process parameters, this condition is achieved after 0.01 seconds of extrusion. It validates a 2D description:

$$\frac{\partial T}{\partial t} = \frac{k_y}{\rho C_p}\frac{\partial^2 T}{\partial y^2} + \frac{k_z}{\rho C_p}\frac{\partial^2 T}{\partial z^2} \quad (20)$$

2.3. Simulation model

In parallel of the experimental measurement, a COMSOL® finite element software was used to solve the 2D transient heat transfer model. The geometry consisting of a stack of rectangles with round corners, according to the one that was printed. The built-in mesher was used with refinement at the rectangle corners.

In order to compare with the pyrometer measurement, the simulated temperature was measured on a point located on the edge of the sixth extruded filament, as shown in

Fig. 7.

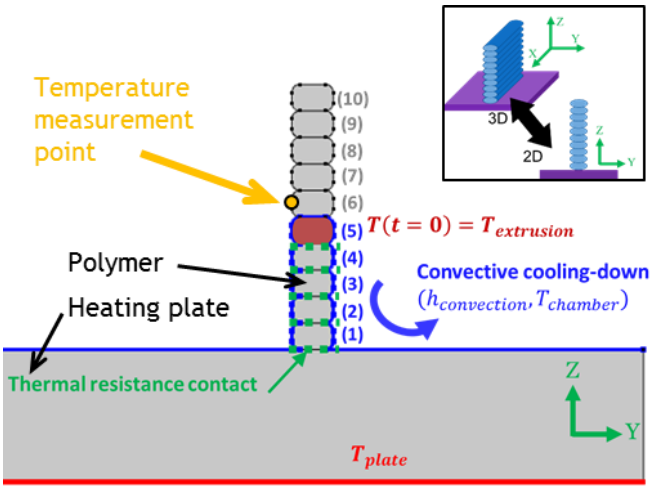

Fig. 7. Model representation, with boundary conditions given for the 5th extruded filament.

The deposition of each filament is simulated leading to a change of geometry and boundary conditions in the numerical model for each new filament. Convective heat transfer is modelled on all interfaces with the air. A constant temperature is imposed at the bottom boundary of the heating plate. Thermal contact resistance is imposed, with a constant value at plate-filament interface and another one at filament-filament interface. New filaments temperature is fixed at $T_{\text{extrusion}}$, as illustrated with

Fig. 7.

A characterization campaign of PEKK thermal properties was performed in our laboratory, for the thermal conductivity k, the specific heat C_p and the density ρ, with the influence of the temperature on the property. For ABS polymer, properties were taken in the bibliography [27]:

Table 1. Thermal properties used for simulations

Property	ABS At 160°C	PEKK At 300°C	Heating plate
Density ρ [kg.m^{-3}]	1050	1140	2210
Specific heat C_p [J.kg^{-1}.K^{-1}]	2100	2200	730
Isotropic thermal conductivity k [W.m^{-1}.K^{-1}]	0.2	0.5	1.4

The process parameters representative of the experimental conditions are given in the following table:

Table 2. Process parameters used for simulation

Parameters	ABS	PEKK
Extrusion temperature (°C)	255	356
Chamber temperature (°C)	95	139
Heating plate temperature (°C)	100	160
Convection coefficient (W.m^{-2}.K^{-1})	30	30
Thermal Contact Resistance on filament-plate interface (m^2.K.W^{-1})	$5{\cdot}10^{-5}$	$5{\cdot}10^{-5}$
Thermal Contact Resistance on filament-filament interface (m^2.K.W^{-1})	10^{-4}	10^{-4}
Time between 2 filaments depositions (s)	8.9	9.8
Filament thickness L_z (m)	$8{\cdot}10^{-4}$	$8{\cdot}10^{-4}$
Filament width L_y (m)	$1.25{\cdot}10^{-3}$	$2.2{\cdot}10^{-3}$

Extrusion, chamber and heating plate temperatures were measured on the experimental bench with 80µm or 250µm K-type thermocouples. Heat transfer coefficient was determined with an empirical correlation for an external free convection flow, with Nusselt number calculated from Rayleigh number [28]. Thermal Contact Resistance (TCR) values were difficult to determine with precision, so low values were given. A sensitivity analysis showed a low influence on the thermal behaviour for those TCR values.

3. Results and discussion

3.1. Qualitative analysis on ABS

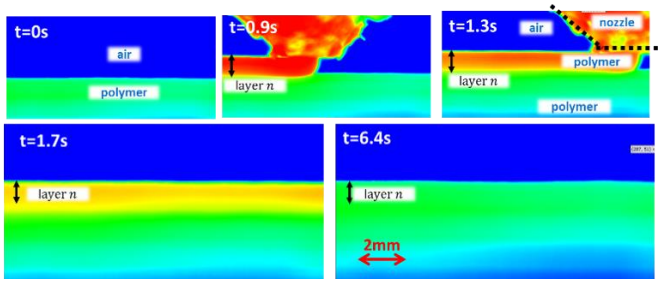

Fig. 8. IR camera qualitative analysis for ABS.

The infrared camera thermal signature is shown in Fig. 8. Each deposited filament can be identified. The temperature gradient in the horizontal direction is much lower than in the vertical direction. Therefore, the conductive heat transfer along the filament length (horizontal axis) can be neglected with respect to the vertical heat transfers. This confirms the approximation proposed in Equations(17)-(19).

3.2. Quantitative analysis on ABS

Thermal history of the filaments was simulated with the properties and process parameters presented in Table 1 and Table 2. The initial time t=0 is considered when the sixth filament is extruded. The temperature field at different times is presented in Fig. 9:

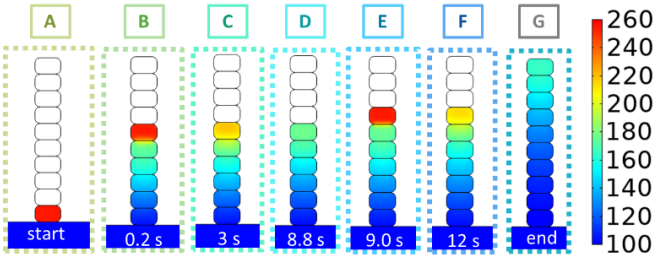

Fig. 9. COMSOL® model giving temperature (°C) evolution for ABS.

The temperature on the edge of the sixth filament is plotted versus time in Fig. 10 with time stamps from Fig. 9 highlighted. Besides, temperature was measured with the pyrometer, approximately on the middle of the length and the height of the part and was aiming the middle of the sixth filament. The measurement was not easy to perform because of the large pyrometer spot (diameter 0.6mm) compared to the filament one (height 0.8mm). Experimental temperatures are compared with numerical predictions and we can observe a very good agreement with a maximum temperature difference of 10°C, but globally less than 5°C.

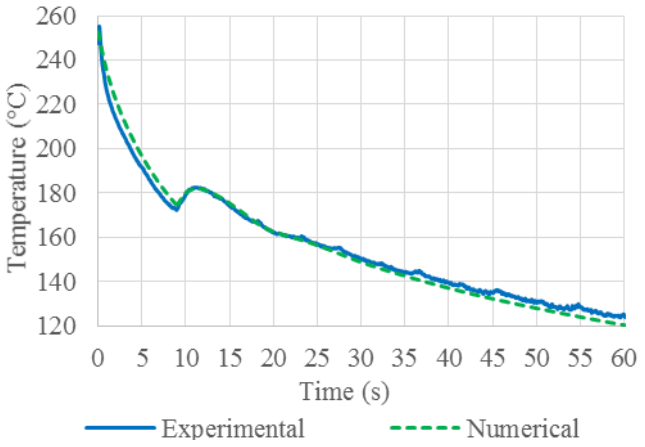

Fig. 10. Pyrometer measurements and simulation comparison for ABS.

Finally, using the experimental temperature evolution, the degree of healing can be calculated. Equation (2) can be solved with an explicit scheme:

$$[H]_{n+1} = \frac{\Delta t}{t_{R(T)}} + [H]_n \quad (21)$$

with $\Delta t = 0.33s$ the time step and $t_r(T)$ the thermo-dependent reptation time

The reptation time dependency with temperature was characterized in the literature by Bartolaï [29] for a printing grade of ABS Ultimachine. Using WLF theory [30], authors gives the temperature dependent reptation time:

$$t_R(T) = t_R(T_{ref}) \cdot exp\left(\frac{-c_1(T-T_{ref})}{c_2+(T-T_{ref})}\right) \quad (22)$$

with $t_R(T_{ref}) = 0.63s$ for $T_{ref} = 210°C$, $C_1 = 4.23$ and $C_2 = 164$.

Degree of healing can be calculated from the experimental temperature profile with Equation (21) and parameters from Equation (22).

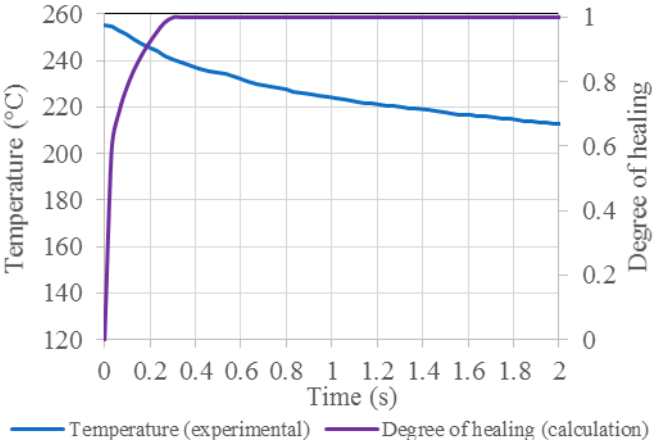

Fig. 11. Degree of healing post-processed from ABS temperature history.

The maximum degree of healing $D_h = 1$ is reached very fast (less than 0.5s). It comes from the rheological properties of the characterized ABS that gives a short reptation time for the ABS processing temperature. Attention must be given to this results. The recommended extrusion temperature for the ABS used in our experiments is 255°C [31], whereas the one characterized in the literature has a recommended extrusion temperature between 215 and 230°C [32]. Therefore those two ABS materials have different viscosities, and probably different reptation times.

3.3. Analysis on PEKK

After this initial study at moderate temperature with ABS, the same experimental and numerical procedure was performed on PEKK material. The processing temperatures are higher, as shown in Table 2.

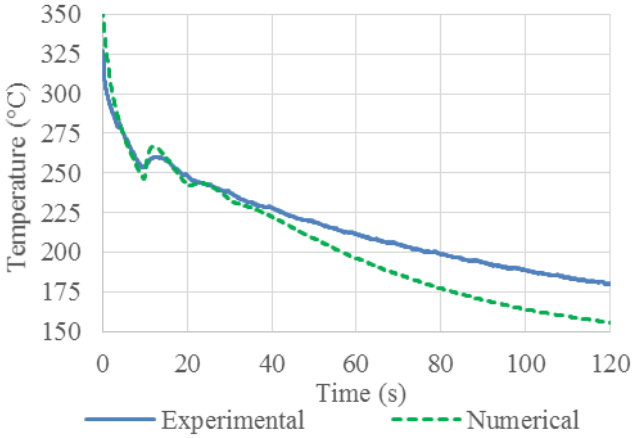

Fig. 12. Pyrometer measurements and simulation comparison for PEKK.

Both temperature evolutions follow the same shape. There is a temperature difference, up to 25°C in the first instants, and from 3s to 50s always less than 10°C. From 50 to 120s, the temperature difference raises to a maximum of 25°C difference that could be explained by a bad control of the heating chamber temperature.

The results presented still need to be improved to decrease the discrepancy between experimental and numerical temperatures. First, a better calibration of the pyrometer

associated with PEKK radiative properties would improve the experimental measurements. And secondly, the simulation may be improved by taking into account temperature-dependent thermal properties and convective heat transfer coefficient. Also, more precise determination of the thermal contact resistance should be carried out.

In order to calculate the degree of healing, PEKK rheological parameters were characterized from another PEKK material grade [33]. The degree of healing is calculated using the experimental temperature evolution and is shown versus time in Fig. 13. It becomes constant after 40 s and is equal to 0.45.

There is an important difference between ABS and PEKK material for FFF process. For ABS, the full healing is reached very fast during the cooling of the filament as shown in Fig. 11. For PEKK, the maximum degree of healing is never reached with the printing conditions usedFig. 13. This shows the importance to characterize accurately the thermo-dependent reptation time of the polymer, and to use a precise prediction of the thermal history undergone by the printed filament. This analysis would determine the process window for a specified material, as shown in Fig. 1.

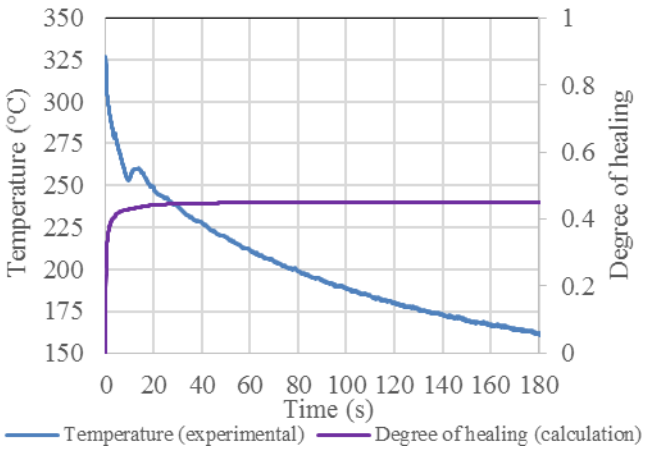

Fig. 13. Degree of healing calculated from PEKK temperature history.

4. Conclusion

This paper aims at predicting the heat transfer and the adhesion behavior during the printing of polymer filament with FFF process. As shown in Fig. 1, temperature history of the filament is the key-element to determine. An experimental instrumented bench was designed and manufactured. It gives *in situ* temperature evolution of the filament. A numerical twin was developed and simulates the transient heat transfer at the filament scale. The calculated temperature field was then post-processed to predict the degree of adhesion.

There is a good adequacy between temperature measured with the pyrometer, and temperature calculated with the COMSOL model. Because of the poor knowledge of the rheological properties, the calculated degree of healing was found to be equal to 1 very quickly for ABS. However, this is the opposite for PEKK material, which reaches only a degree of healing of 0.45 after the cooling-down of the filament.

The bench was designed to handle high temperature and future work will consist in studying deposition of PEKK more precisely, and also for carbon fibers reinforced PEKK with different process parameters.

The short-term perspectives are to use the model with the thermo-dependent thermal properties, which were characterized in the LTeN laboratory on PEKK polymer. Moreover, measurements with the calibrated IR camera need to be performed on the PEKK material. Also, others perspectives would be to study the coalescence evolution in order to predict the macro-porosities formation in the FFF parts production. With those two steps, the coalescence and the healing, a global degree of adhesion would be calculable. This would give precious information about the process window of the FFF process, with high performance composites used for aeronautics applications.

Acknowledgment

This study is part of the FACT project managed by IRT Jules Verne (French Institute in Research and Technology in Advanced Manufacturing Technologies for Composite, Metallic and Hybrid Structures). The authors wish to associate the industrial and academic partners of this project, respectively AIRBUS, ARKEMA, DAHER, DEDIENNE, EOS, LIEBHERR, SAFRAN, ZODIAC Engineering, CANOE, TOBECA, LTeN, PIMM, CNRS, ENSAM and Université de Nantes.

The authors want to thank Gwenaël BIOTTEAU and Nicolas LEFEVRE from the technical service of LTeN laboratory, for their help in the experimental bench design and fabrication.

References

[1] Wohlers TT, Campbell I, Diegel O, Huff R, Kowen J, Wohlers Report 2019. 2019.

[2] Frenkel J, Viscous Flow of Crystalline Bodies under the Action of Surface Tension. J Phys (USSR) 1945; 9(5): 385-91.

[3] Pokluda O, Bellehumeur CT, Machopoulos J, Modification of Frenkel ' s Model for Sintering. AIChE J 1997; 43, (12): 3253–56.

[4] Hopper RW, Coalescence of Two Viscous Cylinders by Capillarity: Part I, Theory. Am Ceram Soc J 1993; 76(12): 2947–52.

[5] Hopper RW, Coalescence of Two Equal Cylinders: Exact Results for Creeping Viscous Plane Flow Driven by Capillarity. Am Ceram Soc J 1984; 67(12): C262–4.

[6] Defauchy D, Simulation du procédé de fabrication directe de pièces thermoplastiques par fusion laser de poudre. PhD thesis 2013, Arts et métiers ParisTech, France.

[7] Sun Q, Rizvi GM, Bellehumeur CT, Gu P, Effect of processing conditions on the bonding quality of FDM polymer filaments. Rapid Prototyp J 2008; 14(2): 72–80.

[8] Bellehumeur C, Li L, Modeling of Bond Formation Between Polymer Filaments in the Fused Deposition Modeling Process. J Manuf Process 2004; 6(2): 170–8.

[9] Kazmer DO, A Protocol for Filament Production and Use in Fused Deposition Modeling. SPE Antec 2016, 881–6.

[10] Faes M, Ferraris E, Moens D, Influence of Inter-layer Cooling time on the Quasi-static Properties of ABS Components Produced via Fused Deposition Modelling. Procedia CIRP 2016; 42: 748–53.

[11] Brenken B, Barocio E, Favaloro A, Kunc V, Pipes RB, Fused filament fabrication of fiber-reinforced polymers: A review. Addit Manuf 2018; 21: 1–16.

[12] Li L, Sun Q, Bellehumeur C, Gu P, Investigation of bond formation in FDM process. Solid Free Fabr Proc 2002; 400–7.

[13] Shahriar BB, Chabert F, Nassiet V, Cantarel A, Garnier C, Toward improvement of the properties of parts manufactured by FFF (fused filament fabrication) through understanding the influence of temperature and rheological behaviour on the coalescence phenomenon. AIP Conference Proceedings 2017; 1896: 040008-1-6.

[14] de Gennes PG, Reptation of a Polymer Chain in the Presence of Fixed Obstacles. J Chem Phys 1971; 55(2): 572–9.
[15] Wool RP, Yuan B-L, McGarel OJ, Welding of polymer interfaces. Polym Eng Sci 1989; 29(19): 1340–67.
[16] Yang F, Pitchumani R, Healing of thermoplastic polymers at an interface under nonisothermal conditions. Macromolecules 2002; 35(8): 3213–24.
[17] Yardimci MA, Güçeri S, Conceptual framework for the thermal process modelling of fused deposition. Rapid Prototyp J 1996; 2(2): 26–31.
[18] Yardimci MA, Danforth S, A phenomenological numerical model for fused deposition processing of particle filled parts. Solid Free Fabr Proc 1995: 189–95.
[19] Thomas JP, Rodriguez JF, Modeling the Fracture Strength Between Fused-Deposition Extruded Roads. Solid Free Fabr Proc 2000: 17–23.
[20] Rodríguez JF, Thomas JP, Renaud JE, Mechanical behavior of acrylonitrile butadiene styrene fused deposition materials modeling. Rapid Prototyp J 2003; 9(4): 219–30.
[21] Shahriar BB, Cantarel A, Chabert F, Nassiet V, Influence of parameters controlling the extrusion step in fused filament fabrication (FFF) process applied to polymers using numerical simulation. AIP Conf. Proc. 2018; 1960: 140003-1-6.
[22] Duty CE, Ajinjeru C, Kishore V, Compton BG, Hmeidat NS, Chen X, Liu P, Hassen AA, Lindahl J, Kunc V, What makes a material printable? A viscoelastic model for extrusion-based 3D printing of polymers., J Manuf Process 2018; 35: 526–37.
[23] Osswald TA, Puentes J, Kattinger J, Fused filament fabrication melting model. Addit Manuf 2018; 22: 51–9.
[24] Heller BP, Smith DE, Jack DA, Effects of extrudate swell and nozzle geometry on fiber orientation in Fused Filament Fabrication nozzle flow. Addit Manuf 2016; 12: 252–64.
[25] Morgan R, Reid R, Baker A, Lucero B, Bernardin J, Emissivity Measurements of Additively Manufactured Materials. Los Alamos National Laboratory report 2017;
[26] Choupin T, Mechanical performances of PEKK thermoplastic composites linked to their processing parameters. PhD thesis 2018, Art et Metiers ParisTech, France.
[27] Thermo-dependant properties of ABS - Gammadot company. NEXUS III Database Thermoplastic Properties. [Online]. Available: http://www.gammadot.com/index.htm?Techzone/nexus/ABS/ABSdatasheet.htm~mainFrame.
[28] Incropera FP, Bergman TL, Lavine AS, DeWitt DP, Fundamentals of Heat and Mass Transfer. 6th ed. John Wiley & Sons, Inc.; 2011.
[29] Bartolai J, Simpson TW, Xie R, Predicting strength of additively manufactured thermoplastic polymer parts produced using material extrusion. Rapid Prototyp J 2017; 24(2): 321–32.
[30] Williams ML, Landel RF, Ferry JD, The Temperature Dependence of Relaxation Mechanisms in Amorphous Polymers and Other Glass-forming Liquids. J Am Chem Soc 1955; 77(14): 3701–7.
[31] Verbatim, Verbatim black ABS - datasheet. [Online]. Available: https://www.verbatim.fr/fr/prod/verbatim-abs-filament-1-75mm-1kg-black-55010/.
[32] Reprap, “Description of ABS used for 3D printing.” [Online]. Available: https://reprap.org/wiki/ABS.
[33] Cender TA, Levy A, Le Corre S, Continuous Welding of High Temperature Thermoplastic Composite Structures. ICMAC Conference 2018.